

Published in final edited form as:

*Dev Cell*. 2014 November 10; 31(3): 319–331. doi:10.1016/j.devcel.2014.08.024.

## B-LINK: A hemicentin, plakin and integrin-dependent adhesion system that links tissues by connecting adjacent basement membranes

Meghan A. Morrissey<sup>1</sup>, Daniel P. Keeley<sup>1</sup>, Elliott J. Hagedorn<sup>1</sup>, Shelly T. H. McClatchey<sup>1</sup>, Qiuyi Chi<sup>1</sup>, David H. Hall<sup>2</sup>, and David R. Sherwood<sup>1,\*</sup>

<sup>1</sup>Department of Biology, Duke University, Science Drive, Box 90388, Durham, NC 27708 USA

<sup>2</sup>Center for *C. elegans* Anatomy, Albert Einstein College of Medicine, 1410 Pelham Parkway, Bronx, NY 10461 USA

### Summary

Basement membrane (BM), a sheet-like form of extracellular matrix, surrounds most tissues. During organogenesis specific adhesions between adjoining tissues frequently occur, however their molecular basis is unclear. Using live-cell imaging and electron microscopy we identify an adhesion system that connects the uterine and gonadal tissues through their juxtaposed BMs at the site of anchor cell (AC) invasion in *C. elegans*. We find that the extracellular matrix component hemicentin (HIM-4), found between BMs, forms punctate accumulations under the AC and controls BM linkage to promote rapid invasion. Through targeted screening we identify the integrin-binding cytolinker plakin (VAB-10A) and integrin (INA-1/PAT-3) as key BM-BM linkage regulators: VAB-10A localizes to the AC-BM interface and tethers hemicentin to the AC while integrin promotes hemicentin punctae formation. Together, plakin, integrin and hemicentin are founding components of a cell-directed adhesion system, which we name a B-LINK (Basement membrane-LINKage), that connects adjacent tissues through adjoining BMs.

### Introduction

Basement membrane (BM) is a conserved, sheet-like extracellular matrix that surrounds most tissues, providing structural support, barrier functions and a surface for signaling activities (Ozbek et al., 2010; Yurchenco, 2011). While the association of BM with cells through structures such as hemidesmosomes and focal adhesions is well established (Yurchenco, 2011), little is known about mechanisms regulating adhesion between BMs of neighboring tissues. Though poorly characterized, connections between juxtaposed BM-encased tissues frequently occur. During organogenesis, for example, the BMs lining the sides of the developing optic cup meet, remodel, and fuse to close the optic fissure (Tsuji et

© 2014 Elsevier Inc. All rights reserved

\*Correspondence: David Sherwood<sup>1</sup> (david.sherwood@duke.edu).

**Publisher's Disclaimer:** This is a PDF file of an unedited manuscript that has been accepted for publication. As a service to our customers we are providing this early version of the manuscript. The manuscript will undergo copyediting, typesetting, and review of the resulting proof before it is published in its final citable form. Please note that during the production process errors may be discovered which could affect the content, and all legal disclaimers that apply to the journal pertain.

al., 2012). BMs also interact to create tight associations between the vasculature and the glomeruli in the kidney and the alveoli in the lung (Abrahamson, 1985; Vaccaro and Brody, 1981) ENREF 3. Further, BM-BM associations underlie formation of the blood-brain barrier, and occur during tumor formation (Hewitt et al., 1992; Ozzello, 1959). These observations suggest that a specific adhesion system might link tissues through neighboring BMs in many important developmental, physiological and disease contexts.

*C. elegans* uterine-vulval attachment is a simple in vivo model to examine the interaction between neighboring BMs (Ihara et al., 2011; Kelley et al., 2014; Sherwood and Sternberg, 2003). Prior to connection, the uterine and vulval tissues are separated by the juxtaposed gonadal and ventral epidermal BMs (Ihara et al., 2011; Sherwood and Sternberg, 2003). The anchor cell (AC), a specialized uterine cell, initiates direct contact with the vulval cells by extending a protrusion that breaches the gonadal and ventral BMs (Sherwood et al., 2005; Sherwood and Sternberg, 2003). Prior to AC invasion, the uterine and vulval tissues shift independently of one another as the animal moves, creating a potential alignment problem during invasion (Sherwood and Sternberg, 2003; Sulston and White, 1980). Whether the AC utilizes a mechanism to stably link the adjacent BMs and fix the position of the uterine and vulval tissues during invasion, is unknown.

One potential candidate for regulating BM-BM interactions is hemicentin (HIM-4), a large (5198-residue) extracellular matrix protein. Hemicentin accumulates between BMs of neighboring organs in *C. elegans*, and its loss leads to defects in the alignment and association between tissues (Vogel and Hedgecock, 2001). Consistent with a possible conserved role in regulating BM-BM interactions, the two hemicentin orthologs in vertebrates also localize between numerous tissues (Xu et al., 2007). Additionally, zebrafish hemicentins regulate the interaction between neighboring epithelia in fin epidermis, as well as the connection between somites and epidermis (Carney et al., 2010; Feitosa et al., 2012). The specific function(s) of hemicentin between tissues, however, is unclear, as it has not yet been possible to dynamically characterize the interactions of BM-encased tissues where hemicentin is found. During *C. elegans* uterine-vulval attachment, hemicentin is secreted by the AC and localizes to punctae in the BM under the AC prior to invasion. In worms lacking hemicentin function, AC invasion is delayed, indicating that hemicentin facilitates invasion (Sherwood et al., 2005). The mechanism by which hemicentin promotes AC invasion, however, is not understood (Hagedorn and Sherwood, 2011).

Using genetic analysis, transmission electron microscopy, tissue shifting experiments and live-cell imaging of BM dynamics during AC invasion we find that the matrix component hemicentin mediates a specific, spatially restricted attachment between the gonadal and ventral BMs under the AC prior to and during invasion. With live-cell imaging we show that this BM-BM linkage is critical for rapid, coordinated invasion through the juxtaposed gonadal and ventral BMs. Through a focused RNAi screen we also identify the plakin isoform VAB-10A (Bosher et al., 2003), which links receptors such as integrin to the cytoskeleton, as a cellular regulator of BM-BM linkage. We show that VAB-10A within the AC is polarized towards the BM, required for BM-BM adhesion, and anchors hemicentin punctae to the region of BM beneath the AC. We also demonstrate that the extracellular matrix receptor integrin (INA-1/PAT-3) is required for the assembly of hemicentin punctae

and BM-BM linkage. Finally, we reveal a similar BM-BM connection that appears to link the uterine utse and epidermal seam cells together, fastening the uterine tissue to the epidermis. Together, these data reveal founding members of an adhesion system we name a B-LINK (for Basement membrane LINKage), which forms a cell-directed connection between the BMs of neighboring tissues.

## Results

### A BM-BM linkage forms specifically under the AC prior to invasion

AC invasion is precisely timed and coordinated with divisions of the underlying P6.p vulval precursor cell and its descendants (Sherwood and Sternberg, 2003). AC invasion initiates at the late P6.p two-cell stage, and is completed approximately 90 minutes later during the P6.p four-cell stage. To determine how the AC invades across the neighboring gonadal and ventral BMs (Figure 1A), we first examined the association of these BMs under the AC using a functional GFP translational fusion of the lone laminin  $\beta$ -subunit (laminin::GFP), whose localization is indistinguishable from immunolocalized laminin (Kao et al., 2006; Sherwood and Sternberg, 2003). The gonadal and ventral BMs are usually tightly juxtaposed and cannot be resolved by light microscopy. In rare cases, however, we observed worms in which the uterine and vulval tissues were slightly separated allowing resolution of each BM. Approximately two hours prior to BM breach, (P6.p one- and early two-cell stage) we were able to identify the ventral and gonadal BM as individual, unattached structures (n=7/9 animals; Figure 1B). This is consistent with observations that the uterine and vulval tissues slide independently at this time (Sulston and White, 1980). During the P6.p two-cell stage, however, more animals showed BM-BM linkage, (13/24 animals; Figure 1B). By the late P6.p two-cell stage (when the AC initiates invasion) most animals had BM-BM linkage under the AC (4/6 animals). Following invasion (P6.p four-cell to P6.p eight-cell stage), the gonadal and ventral BMs fused at the edge of the BM breach created by the AC (n=19/19; Figure 1B) (Ihara et al., 2011). These observations suggest that the two BMs are connected prior to invasion.

To further examine if the BMs might be connected prior to invasion, we photobleached 1-2 micron wide landmarks in the region of the juxtaposed BMs under the AC. Following photobleaching, we laterally slid the worms to induce transient misalignment between the uterine and vulval tissues. This optical marking strategy allowed us to determine whether the bleached regions of BM remained juxtaposed (implicating linkage) or separated (indicating lack of connection). During the P6.p one-cell stage, the bleached regions of BM could shift relative to one another (n=4/8 animals; Figure 1C). In contrast, at the mid P6.p two-cell stage, the bleached regions of BM remained aligned (n=9/9,  $p < 0.05$  compared to P6.p one-cell stage, Fisher exact test; Figure 1C). These optical highlighting experiments further support the idea that the uterine and vulval BMs become linked under the AC prior to invasion.

We hypothesized that the BMs could fuse into a single sheet or remain two distinct sheets held together by an adhesive structure. To distinguish between these possibilities, we examined the BM beneath the AC using transmission electron microscopy. We cut longitudinal serial sections across the entire width of the gonad, allowing us to use the

surrounding tissue to identify the AC and establish the precise developmental stage of the worm. Electron micrographs revealed punctate electron dense structures between the gonadal and ventral BMs prior to invasion (n=4/5 animals, P6.p two-cell stage; Figure 1D and S1). These structures spanned the space between the gonadal and ventral BMs and had an average width of  $130\pm 10$  nm ( $\pm$ SEM, n=5 punctae with entire structure visible). Thus, prior to invasion, the gonadal and ventral BMs become linked under the AC by an adhesive structure.

### **Hemicentin is present at the site of BM-BM adhesion**

We were next interested in determining the molecular mechanism of BM-BM adhesion. Because hemicentin is secreted by the AC prior to invasion and is known to localize between BMs, we hypothesized that hemicentin might link the BMs under the AC (Sherwood et al., 2005). To determine if hemicentin secretion correlates with the time of BM-BM adherence, we examined hemicentin localization using a functional GFP tagged hemicentin (GFP::hemicentin) (Vogel and Hedgecock, 2001). Hemicentin was deposited at low levels throughout the ventral and gonadal BMs, and accumulated in track-like lines at the edges of the ventral BM (Figure 2A). Notably, prior to invasion (From P6.p one-cell stage to mid P6.p two-cell stage), hemicentin accumulated in punctae precisely under the AC (Figures 2A, 2B and S2). The approximate size of the hemicentin structures was similar to the size of the BM-BM adhesions observed with electron microscopy ( $187.2\pm 0.8$  nm, n=104 structures in 23 worms; Figure S2). Time-lapse imaging revealed that hemicentin structures were static and new punctae continued to form throughout the course of AC invasion. Once formed, the hemicentin structures remained within the BM under the AC and did not disassemble during invasion (n=132 punctae in 22 animals; Figure 2B; Movie S1). Optical highlighting of the BM components laminin and type IV collagen has recently shown that the AC physically displaces BM during invasion (Hagedorn et al., 2013). Consistent with a strong association with the BM, the hemicentin punctae were also physically displaced by the invading AC (Figure 2A; Movie S2). Thus, hemicentin punctae are tightly associated with the BM and are present at the time and location of BM-BM adherence.

### **BM-BM adhesion is hemicentin dependent**

To determine if hemicentin plays a role in BM-BM adhesion, we analyzed the gonadal and ventral BMs in animals harboring a null mutation in hemicentin (*him-4(rh319)*) (Vogel and Hedgecock, 2001). In contrast to wild-type animals, the BMs beneath the AC could be independently resolved prior to and during invasion (n=10/10 animals; Figure 2C and 2D), suggesting that the specific linkage between the BMs is lost in hemicentin mutants. Interestingly, the BMs still fused into a continuous sheet following invasion, indicating that BM fusion is not dependent on hemicentin (n=10/10 animals; Figure 2C).

To further examine the role of hemicentin in BM-BM linkage, we performed tissue-shifting experiments. In contrast to wild-type animals, loss of hemicentin allowed the gonadal and ventral BMs to shift beneath the AC at the P6.p two-cell stage (n=3/4,  $p<0.05$  compared to wild-type, Fisher's exact test; compare Figure 1C and 2E). Furthermore, electron microscopy revealed that the structures spanning the BMs underneath the AC were no

longer present in *him-4(rh319)* mutants (n=4/4 ACs at the P6.p two-cell stage; Figure 2F). We conclude that hemicentin is required for BM-BM adhesion.

### AC invasion is delayed when BM-BM adhesion is disrupted

To explore the role of hemicentin and BM-BM adhesion in invasion, we visualized BM removal during AC invasion, utilizing time-lapse analysis from the ventral perspective for increased resolution (Hagedorn et al., 2013). We found that wild-type animals usually breached the gonadal and ventral BMs before widening a gap in both BMs (n=6/10 time-lapsed animals; Figure 3A). While hemicentin mutants (*him-4(rh319)*) initiated invasion at the same time as wild-type animals, they initially breached only the gonadal BM, and widened the gap in the gonadal BM alone (n=10/10 time-lapsed animals; Figure 3A and S3). *him-4(rh319)* mutants eventually breached the ventral BM, but in a delayed manner (Figure 3B; Movie S3). To further quantify the extent of this defect, we assessed ventral BM breach in relation to the size of gonadal BM breaches. We found that in worms with gonadal BM breaches between 1-5  $\mu\text{m}^2$  in area (the smallest detectable size), the majority of wild-type animals had already breached both BMs (Figure 3C). In contrast, only a few *him-4(rh319)* mutants with similarly sized gonadal BM breaches had breached both BMs (Figure 3C). Further, in worms with larger gonadal BM gaps (10-25  $\mu\text{m}^2$ ), only 67% of hemicentin mutant worms breached the ventral BM, while all wild-type worms had breached both BMs (Figure 3C). Notably, ACs lacking hemicentin opened the gonadal BM at approximately half the rate that wild-type worms opened both BMs (Figure 3D and 3E). Once the AC of hemicentin mutants initiated ventral BM breach, the ventral BM gap opened quickly (Figure 3B, 3D and 3E; Movie S3). Our data suggests that removing hemicentin eliminates BM-BM adhesion and that this adhesion is required for efficient invasion.

Our tissue shifting, TEM and visual analysis suggested that removing hemicentin completely eliminates BM-BM adhesion and that this adhesion is required for efficient invasion. To test the idea that the hemicentin dependent BM-BM linkage promotes efficient invasion, we examined genetic interactions between hemicentin and the netrin receptor UNC-40/DCC. Loss of *unc-40* results in a delay in invasion from a distinct invasion defect--an inability to generate a protrusion that crosses the basement membrane (Hagedorn et al., 2013). We hypothesized that if the hemicentin dependent BM-BM adhesion promotes efficient invasion, the defect in invasion would be dramatically enhanced in animals harboring mutations in both *him-4* (hemicentin) and *unc-40*. Supporting this idea, AC invasion was nearly abolished in *unc-40; him-4* double mutant animals (93% failed to invade in *unc-40(e271); him-4(rh319)* versus 43% in *unc-40(e271)*; n=28 and 58 respectively; p<0.0005). Thus hemicentin and BM-BM adhesion promote rapid, coordinated breaching and clearance of the gonadal and ventral BMs.

### VAB-10A (plakin) promotes BM-BM adhesion

Previous work in *C. elegans* has shown that hemicentin is required to organize hemidesmosomes in the epidermis around the mechanosensory neurons and the utse syncytium (Vogel and Hedgecock, 2001). Because hemicentin might be a structural component of both hemidesmosomes and BM-BM adhesions, we hypothesized that other components of hemidesmosomes may function in BM-BM attachment (Vogel and

Hedgecock, 2001). To identify possible additional components of the BM-BM adhesion system, we performed a targeted screen examining mutant alleles or RNAi mediated knockdown of genes associated with hemidesmosomes for defects in AC invasion or hemicentin punctae formation (Table 1, S1 and S2; (Carbon et al., 2009). From this screen, we identified two genes as potential regulators of AC invasion, *vab-10* and *mua-3*. A missense mutation in *vab-10* (*vab-10(e698)*) (Bosher et al., 2003) had a 35% invasion defect (n=56; Table 1), which is similar to the invasion defect caused by loss of hemicentin (*him-4(rh319)*). In contrast, RNAi-mediated knockdown of *mua-3* caused a less penetrant defect (11% invasion defect, p<0.05, n=65; Table 1) and the only viable *mua-3* allele, which disrupts hypodermal hemidesmosomes (Bosher et al., 2003), did not affect AC invasion. Additionally, RNAi targeting *mua-3* did not appear to cause a defect in BM-BM adhesion, as 86% of worms penetrated both BMs before widening the gap (n=14 worms with gonadal BM breaches 1-5 $\mu$ m<sup>2</sup> in area). We thus focused on the role of *vab-10*.

The gene *vab-10* is the sole *C. elegans* plakin locus and encodes multiple isoforms, the most abundant of which are *vab-10a* and *vab-10b* (Bosher et al., 2003). The *vab-10(e698)* allele, which results in an AC invasion defect, specifically affects the *vab-10a* isoform and not the *vab-10b* isoform (Bosher et al., 2003). VAB-10A structurally resembles the epithelial plakins and is most closely homologous to plectin although VAB-10A lacks the microtubule-binding domain found in vertebrate plectin (Bosher et al., 2003; Jefferson et al., 2004). RNAi targeting *vab-10a* produced a similar reduction in invasion efficiency, providing further support that *vab-10a* plays a role in AC invasion (Table 1). Genetic loss of *vab-10b* is embryonic or early larval lethal (Bosher et al., 2003). We thus utilized RNAi to target *vab-10b* during mid-larval stages, and found that reduction of *vab-10b* did not significantly affect AC invasion (Table 1). Together, this data suggests that the *vab-10a* isoform promotes AC invasion.

To determine if VAB-10A (plakin) plays a role in BM-BM adhesion, we examined worms in which the gonadal and vulval tissues were slightly separated, allowing independent resolution of the gonadal and ventral BMs. Similar to hemicentin mutants, the BMs were resolvable after treating with RNAi targeting *vab-10a* just prior to invasion, indicating an absence of adhesion between the two BMs (Figure 4A). To confirm that VAB-10A plays a role in linking BMs during AC invasion, we assayed worms for a delay in breaching the ventral BM following *vab-10a* knockdown. As in hemicentin mutants, we found that RNAi knockdown of *vab-10a* resulted in a specific delay in breaching the ventral BM (Figure 4B). Importantly, invadopodia, which are F-actin rich structures within the AC that mediate BM breaching (Hagedorn et al., 2014; Hagedorn et al., 2013), were not affected by loss of *vab-10a* (Figure S4). These results suggest that VAB-10A regulates AC invasion by promoting BM-BM adhesion.

To better understand how VAB-10A controls BM-BM adherence, we examined the localization of the VAB-10A protein during AC invasion. We used the CRISPR-Cas9 system of genome editing (Dickinson et al., 2013) to insert GFP directly into the last exon of *vab-10a*, which is not shared with the other major *vab-10* isoform, *vab-10b* (Bosher et al., 2003). The GFP insertion revealed a high concentration of VAB-10A::GFP in circumferential bands in the epidermis, consistent with immunolocalization of VAB-10A

(Bosher et al., 2003). Additionally, we observed that *vab-10a* was enriched at the invasive cell membrane of the AC (Figure 4C and S5), suggesting that VAB-10A functions within the AC at the invasive membrane to promote BM-BM adhesion. To directly test whether VAB-10A functions within the AC, we used a *C. elegans* strain in which only uterine tissue, including the AC, is sensitive to RNAi (Hagedorn et al., 2009). We found that knocking down *vab-10a* only in the uterine cells led to a 34% invasion defect, similar to the invasion defect caused by whole-body *vab-10a* knockdown (Table 1). In contrast, knocking down *vab-10a* in a strain where only the vulval cells are sensitive to RNAi did not significantly affect invasion (Table 1). Furthermore, expression of *vab-10a::GFP* specifically within the AC rescued the invasion defect of the *vab-10* mutant (Table 1; Figure 4D). We conclude that VAB-10A functions within the AC to regulate BM-BM adhesion.

VAB-10A connects hemidesmosome-like fibrous organelles to the intermediate filament cytoskeleton in the *C. elegans* epidermis (Bosher et al., 2003). To determine if VAB-10A might similarly connect the hemicentin based BM-BM adhesions to intermediate filaments, we conducted a preliminary RNAi screen examining each of the 11 intermediate filament genes for AC invasion defects, followed by a more extensive targeted screen in the RNAi sensitive *rrf-3(pk1426)* strain (Table S3 and Table 1). RNAi mediated knockdown of IFC-2, IFD-1 and IFD-2 individually produced few AC invasion defects, however, when IFC-2, IFD-1 and IFD-2 were reduced in combination, the number of AC invasion defects increased, suggesting these proteins may function redundantly to promote invasion (Table 1). To more directly test if VAB-10A requires intermediate filaments to function in the AC, we created transgenic animals with an AC-expressed form of VAB-10A lacking all plectin repeat domains, which are responsible for intermediate filament binding (*cdh-3>vab-10a PRD::GFP*). Similar to full length VAB-10A, VAB-10A PRD was enriched at the invasive membrane (Figure S4), however, VAB-10A PRD was not able to rescue AC invasion in the *vab-10(e698)* background (Table 1). Taken together, this data suggests that VAB-10A might mediate a connection between the hemicentin dependent BM-BM adhesions and intermediate filament proteins in the AC.

### VAB-10A (plakin) anchors hemicentin punctae under the AC

Reduction of *vab-10a* (plakin) and loss of *him-4* (hemicentin) resulted in similar defects in BM-BM linkage, suggesting that they function together to link the gonadal and epidermal BMs under the AC. To further test this notion, we examined genetic interactions between both genes. If *him-4* and *vab-10a* operated in the same genetic pathway to promote BM-BM adhesion, loss of *vab-10a* would not be expected to increase the invasion defect of *him-4(rh319)* animals. Consistent with this notion, RNAi depletion of *vab-10a* in *him-4(rh319)* worms did not enhance the AC invasion defect (Table 1).

To understand how hemicentin and VAB-10A might cooperate to regulate BM adherence, we next analyzed the effect of *vab-10a* RNAi on hemicentin localization. After *vab-10a* knockdown, hemicentin was still secreted and formed punctae in the BM under the AC. Unlike wild-type animals, however, where hemicentin punctae remained in the BM under the AC, we noted a change in hemicentin localization. In worms treated with *vab-10a* RNAi hemicentin aggregates were no longer restricted to the footprint of the AC (Figure 4E and

4F). In contrast, treating worms with *him-4* RNAi did not effect VAB-10A::GFP localization (n=11/11 animals; Figure S4). Together, these data suggest that VAB-10A regulates BM-BM adhesions by indirectly anchoring hemicentin punctae to the region of BM beneath the AC.

### Integrin is required to assemble hemicentin punctae

The presence of an intracellular component (VAB-10A) and an extracellular component (hemicentin) required for BM-BM linkage under the AC suggested that a transmembrane receptor was also likely a requirement. We thus screened all known BM receptors in *C. elegans* for AC invasion defects using a combination of RNAi treatment, mutant analysis and previously published data (Hagedorn et al., 2009; Ziel et al., 2009) to identify AC invasion defects (Table S3). While mutations or RNAi targeting most of the BM receptors did not affect AC invasion, RNAi targeting either subunit of the INA-1/PAT-3 integrin dimer disrupted AC invasion (Table S3). Like VAB-10A, integrin is enriched along the entire AC-BM interface, suggesting that integrin and VAB-10A both localize to the AC-BM interface adjacent to the extracellular hemicentin punctae (Figure S5). Reducing the function of integrin results in a failure to form invadopodia that breach the BM, causing a highly penetrant invasion defect (Hagedorn et al., 2009). Consistent with a separate role in BM-BM linkage, integrin is required for the formation of hemicentin punctae, but not for hemicentin transcription (Hagedorn et al., 2009). To determine how integrin regulates hemicentin deposition, we examined hemicentin accumulation after the specific disruption of integrin activity in the AC using a previously characterized AC-specific dominant-negative integrin construct (*zmp-1>HA-βtail*; (Hagedorn et al., 2009). Notably, hemicentin did not accumulate intracellularly, indicating that integrin is not required for hemicentin secretion (n=10/10 animals observed; Figure 5A). Furthermore, hemicentin was not deposited inappropriately along the lateral membrane of the AC, which occurs when AC polarity is disrupted (Morf et al., 2013; Ziel et al., 2009). Increased levels of hemicentin, however, were found diffusely in the surrounding BM under the AC (Figure 5A, 5B and S5). This suggests that integrin activity is required for punctae formation at the site of BM-BM adherence, but not for general secretion or deposition in the BM. Additionally, integrin has been shown to bind to the VAB-10A homolog plectin in vertebrates (Rezniczek et al., 1998), thus we hypothesized that integrin might also be required for VAB-10A localization. Consistent with this, loss of integrin function in the AC (*zmp-1>HAβtail*) disrupted the polarized localization of VAB-10A along the AC-BM interface and resulted in diffuse VAB-10A throughout the cytoplasm (compare Figure 5C with 4C). Together, this data suggests that integrin is required to connect both hemicentin and VAB-10A to the site of BM-BM adhesion. To determine if integrin regulates BM-BM adherence, we assayed worms treated with *ina-1* RNAi for a delay in breaching the ventral BM relative to gonadal BM breach. Similar to loss of hemicentin and *vab-10a*, we found that following RNAi-mediated knockdown of *ina-1* there was a delay in breaching the ventral BM (Figure 5D). Taken together, these data suggest that integrin regulates the formation and function of the BM-BM adhesion under the AC.



## Hemicentin, VAB-10A and integrin mediate utse-seam cell connection

We next wanted to determine if hemicentin, VAB-10A and integrin link adjacent BMs in other contexts. We thus examined the BM-BM connection between the uterine utse and hypodermal seam cell, a linkage that helps maintain the uterus inside the animal during egg-laying (Figure 6A) (Newman et al., 1996; Vogel and Hedgecock, 2001). Notably, hemicentin localizes to the site of BM-BM attachment and eliminating hemicentin causes the utse and the seam cell to separate between their BMs, resulting in uterine prolapse or rupture through the vulva (Vogel and Hedgecock, 2001). Importantly, we found that in addition to hemicentin, VAB-10A and integrin were enriched at the site of utse and seam cell attachment (Figure 6B). Further, RNAi knockdown of *vab-10a* or *ina-1* (integrin) in either the entire worm or specifically in the uterine tissue resulted in uterine prolapse (Figure 6C and 6D). Together, these results indicate that regulators of BM-BM adhesion under the AC also control the linkage between the BMs surrounding the utse and the seam cell.

## Discussion

Utilizing electron microscopy, live-cell imaging, and focused screening in *C. elegans* we identify here a cell-directed BM-BM adhesion system, which we name a B-LINK (Basement membrane-LINKage), that links tissues through their adjoining BMs (Figure 6E). Notably, the molecular regulators of this adhesion system--hemicentin, plakin and integrin--are highly conserved. The widespread observation of connections between juxtaposed BMs and the conserved nature of the components suggests B-LINKs might be broadly utilized to attach adjacent tissues through BMs.

Previous research has indicated that the extracellular matrix protein hemicentin is required to mediate interactions between BM-lined tissues in *C. elegans* and zebrafish larvae (Carney et al., 2010; Feitosa et al., 2012; Vogel and Hedgecock, 2001). Further suggesting a conserved function between BMs, the two mouse hemicentins are localized between tissues that undergo mechanical stress (Xu et al., 2007). The exact function of hemicentin in these cases, however, has remained unclear because the timing of hemicentin activity and the exact nature of its role between BMs have been difficult to establish. We show here that the *C. elegans* gonadal anchor cell (AC) secretes hemicentin into the BM just prior to its invasion into the vulva. Using tissue shifting experiments and live-cell imaging we find that hemicentin punctae link the juxtaposed gonadal and ventral BMs to facilitate the AC's rapid and coordinated invasion through these BMs—a process critical for initiating direct uterine-vulval connection (Sherwood and Sternberg, 2003). Given that hemicentin is known to predominantly localize between BMs (Vogel and Hedgecock, 2001), hemicentin may act as a direct bridge between the gonadal and ventral BMs. Hemicentin contains an N-terminal von Willebrand A (VWA) domain, which has been proposed to bind collagen (Whittaker and Hynes, 2002), and several self-association sites, including the multiple tandem epidermal growth factor (EGF) domains and the fibulin-like carboxy terminus (Dong et al., 2006). Thus, hemicentin may be capable self-associating into aggregates that bind both BMs.

The *C. elegans* VAB-10A protein is a plakin most closely related to vertebrate plectin, a highly versatile cytolinker that connects transmembrane receptors to the cytoskeleton in

cells (Bosher et al., 2003; Jefferson et al., 2004). Our data indicate that VAB-10A is required within the AC to form a functional B-LINK. In the absence of VAB-10A, hemicentin is still secreted and accumulates into punctae, but the structures cannot hold together the uterine and vulval tissues. VAB-10A might act in part to tether hemicentin to the AC, as reducing VAB-10A results in hemicentin punctae outside the AC footprint. In both vertebrates and *C. elegans*, plectin and VAB-10A have been implicated in linking transmembrane receptors to the intermediate filament cytoskeleton (Bosher et al., 2003; Rezniczek et al., 1998). Because the intermediate filament-binding domain of VAB-10A is required for VAB-10A function in the B-LINK, VAB-10A may function to connect the B-LINK to the intermediate filament network. Interestingly, the plectin (VAB-10A) knockout mouse exhibits defects in muscle attachment and destabilized hemidesmosomes in the epidermis, suggesting a conserved role for plectin in strengthening cell-matrix adhesion (Andra et al., 1997).

Our studies also point to a role for integrin in BM-BM adhesion, as the integrin heterodimer INA-1/PAT-3, which is most similar to vertebrate laminin binding integrins (Baum and Garriga, 1997), is required to establish hemicentin punctae, recruit VAB-10A and form a functional BM-BM linkage. A vertebrate homolog of VAB-10A, plectin, is known to directly interact with  $\alpha_6\beta_4$  integrin, a laminin-binding integrin present at hemidesmosomes (Rezniczek et al., 1998; Seifert et al., 1992). Additionally, the *Drosophila* plakin *short stop*, functions with PS integrins to mediate adhesion between muscle and epidermal tissues (Gregory and Brown, 1998; Roper et al., 2002). The conservation of integrin association with plectin, and role of INA-1/PAT-3 in hemicentin punctae formation, suggests that integrin may not only be required for B-LINK formation but also to anchor B-LINKs to the AC's cytoskeleton.

The B-LINK may represent a developmental switch in matrix function from a protective layer that facilitates tissue sliding to an adhesive link between tissues. Suggesting that the B-LINK may additionally reflect a common strategy for stably linking BMs, we found that the B-LINK components are required to connect the uterine seam cells. In *C. elegans*, the muscle and epidermis are also connected through an intervening matrix (Bosher et al., 2003; Labouesse, 2012). Molecularly, this attachment, referred to as a fibrous organelle (FO) has similarities to a B-LINK, including a requirement for VAB-10A and intermediate filaments, but also important distinctions from the B-LINK (Bosher et al., 2003; Labouesse, 2012). For example, alleles of *vab-19* and *mua-3* that affect the FO do not disrupt the B-LINK (Table 1) (Bercher et al., 2001; Ding et al., 2003) and hemicentin, a critical component of the B-LINK, is not localized to FOs nor required for FO function. Intriguingly, the matrix-spanning attachment between the muscle and epidermis is required to transmit signals from the muscle to the epidermis, reinforcing cell-matrix adhesion in response to mechanical signals from the muscle (Zhang et al., 2011). Thus it will be interesting to examine if the B-LINK provides more than a physical connection between tissues.

We expect that BM-BM adhesion is a common mechanism for coordinating interactions between neighboring tissues. BM-BM adhesion structures are likely important when BM lined tissues fuse to form a single structure, as occurs in optic cup development (Tsuji et al., 2012), when invasive cells must traverse juxtaposed BMs, as happens during AC invasion in

*C. elegans* and *Drosophila* wing disc eversion (Srivastava et al., 2007), or when two BMs are tightly juxtaposed, such as in kidney glomeruli and lung alveoli (Kefalides and Borel, 2005; Vaccaro and Brody, 1981). Interestingly, zebrafish models implicate hemicentin as a potential regulator of Fraser Syndrome, a developmental disorder caused by transient BM defects and epithelial blistering (Carney et al., 2010). Mutations in human hemicentin are associated with macular degeneration, which is frequently caused by disruption of Bruch's membrane, a structure that originates as two juxtaposed BMs (Booij et al., 2010; Carney et al., 2010; Thompson et al., 2007). The molecular identification of the B-LINK might thus have important implications in numerous developmental events, tissue structures and human pathologies where BM-BM adhesions regulate organ construction and tissue functions.

## Experimental Procedures

### Strains and Culture Conditions

Culturing and handling of *C. elegans* was performed as previously described (Brenner, 1974). Wild-type animals were strain N2. In the text and figures, we designated linkage to a promoter with a (>) symbol and use a (::) symbol for linkages that fuse open reading frames. The following alleles and transgenes were used in this study: qyIs102(*fos-1a*>*rde-1*); qyIs127(*laminin::mCherry*); *rol-6*(*su1006*); *urIs*(*rol-6*(*su1006*), *laminin::GFP*); qyEx459(*cdh-3*>*vab-10a* PRD::*GFP*, *myo-2::GFP*); qyEx460(*cdh-3*>*vab-10a* PRD::*GFP*; *unc-119(+)*) **LG I** *vab-10*(*ju281*); **LG II** *rff-3*(*pk1426*); qyIs23[*cdh-3*>*mCherry::PLCδ<sup>PH</sup>*]; *vab-19*(*e1036*); **LG III** *unc-119*(*ed4*), *rhIs23*[*GFP::hemicentin*]; *syIs129*( SP-*GFP-hemicentin*); *mua-3*(*rh195*) **LG IV** *mfls70*(*lin-31*>*rde-1*); qyIs10[*laminin::GFP*]; *eps-8*(*ok539*); qyIs42[*pat-3::GFP*; genomic *ina-1*]; qyIs15[*zmp-1*> HA-β -tail ]; **LG V** *rde-1*(*ne219*); qyIs50[*cdh-3*>*mCherry::moeABD*]; **LG X** *him-4*(*rh319*); *pak-1*(*ok448*); *pix-1*(*gk416*); *git-1*(*tm1962*).

### Light Microscopy, Image Acquisition, Processing and Analysis

Images were acquired using a Hamamatsu EM-CCD camera and a Yokogawa CSU-10 spinning disk confocal mounted on a Zeiss AxioImager microscope with a 100× Plan-Apochromat objective. The microscope was controlled by iVision software (Biovision Technologies, Exton, PA) or microManager (Edelstein et al., 2010). Acquired images were processed to enhance brightness/contrast using ImageJ 1.40g and Photoshop (CS6 Extended Adobe Systems, Inc., San Jose, CA), and smoothed using a 0.8 pixel radius Gaussian blur filter. 3D reconstructions were built from confocal Z-stacks, analyzed, and exported as (.mov) files using IMARIS 7.4 (Bitplane, Inc., Saint Paul, MN). Figures and graphs were constructed using Illustrator (CS3 Extended Adobe Systems, Inc., San Jose, CA) and JMP (Version 10, SAS Institute Inc., Cary, NC, 1989-2007). Movies were annotated using Photoshop. Timelapse imaging and invadopodia analysis was performed as described previously (Hagedorn et al., 2013).

### Electron Microscopy

L3 worms were fixed and embedded for serial sectioning as previously described (Hall et al., 2012). Images were acquired on a Phillips CM12. The transverse section in Figure S1 is

part of an archival series originally collected in the laboratory of Sydney Brenner (MRC/LMB, Cambridge, England) and now curated by the Hall lab.

### Landmark photobleaching and tissue shifting

Worms were photobleached on an inverted Zeiss LSM 510 confocal equipped with a 100x Plan-Apochromat objective. Regions of interest were bleached using 500 iterations of a 488 Argon/2 laser at 100% power. Worms were then imaged on the Yokogawa CSU- 10 spinning disk confocal, moved approximately 1mm across the agar pad by sliding the coverslip along the longitudinal axis of the worm, and imaged again to detect a transient shift in tissue alignment.

### Uterine-vulval tissue separation

Worms were incubated on 5% agar with 0.01M NaN<sub>3</sub> for up to one hour. Under these conditions, the uterine and vulval tissues will occasionally separate, allowing visualization of the distinct BMs. To measure the average distance between the BMs, the BMs were traced in ImageJ and connected by perpendicular lines. The area of the resulting rectangle was divided by the Feret's diameter, which was assumed to approximate the width of the rectangle.

### Analysis of AC invasion and hemicentin punctae

The efficiency of AC invasion was analyzed at the P6.p four-cell stage as previously described (Sherwood and Sternberg, 2003). Worms were staged using a combination of divisions of P6.p and the ventral uterine cells, distal tip cell migration, and development of the surrounding tissues. Invasion was scored as "complete invasion" if the BM was removed beneath the AC, "partial invasion" if the BM was breached but not cleared beneath the AC, and "no invasion" if there was no BM breach. The area of BM breach was measured in ImageJ by creating a maximum projection from a ventral perspective confocal z-stack and using an intensity threshold to select the area of gonadal BM breach as indicated by decreased laminin::GFP signal.

To measure the volume of GFP::hemicentin punctae, 3D reconstructions of the AC-BM interface were made from confocal z-stacks. Isosurface renderings of GFP::hemicentin were created by setting a consistent threshold fluorescence intensity value such that the diffuse BM signal was excluded, but the bright hemicentin punctae were not. The line-shaped structures on either side of the ventral BM were excluded from our analysis as they appear to represent a different population of hemicentin. Quantitative measurements of hemicentin volume were performed in Imaris 7.4.

### Statistical Analysis

All statistical analysis was performed in JMP version 9.0 (SAS Institute), using either a two-tailed unpaired Student's *t* test, a Wilcoxon Rank-Sum test or a two-tailed Fischer's exact test. Confidence intervals reported are 95% confidence intervals with a continuity correction. Figure legends specify which test was used.

## Supplementary Material

Refer to Web version on PubMed Central for supplementary material.

## Acknowledgments

We thank N. Medvitz and S. Miller at Duke Electron Microscopy Services; K. Nguyen at the Center for *C. elegans* Anatomy; B. Vogel and M. Labouesse for strains and discussions, and L. Kelley, L. Lohmer, D. Matus, and J. Pelton for comments on the manuscript. Some strains were provided by the CGC, which is funded by NIH Office of Research Infrastructure Programs (P40 OD010440). The TEM image shown in Figure S1 comes from the laboratory of Sydney Brenner at MRC/LMB in Cambridge England, provided courtesy of John White and Jonathan Hodgkin. Curation of the Brenner EM archive in David Hall's lab in NY is supported by NIH grant OD010943 to D.H. This work was supported by The Pew Scholars Program in the Biomedical Sciences and NIH Grants GM079320 and GM100083 to D.R.S.; and an NSF Graduate Research Fellowship to M.A.M.

## References

- Abrahamson DR. Origin of the glomerular basement membrane visualized after in vivo labeling of laminin in newborn rat kidneys. *Journal of Cell Biology*. 1985; 100:1988–2000. [PubMed: 3889015]
- Andra K, Lassmann H, Bittner R, Shorny S, Fassler R, Propst F, Wiche G. Targeted inactivation of plectin reveals essential function in maintaining the integrity of skin, muscle, and heart cytoarchitecture. *Genes Dev*. 1997; 11:3143–3156. [PubMed: 9389647]
- Baum PD, Garriga G. Neuronal migrations and axon fasciculation are disrupted in *ina-1* integrin mutants. *Neuron*. 1997; 19:51–62. [PubMed: 9247263]
- Bercher M, Wahl J, Vogel BE, Lu C, Hedgecock EM, Hall DH, Plenefisch JD. *mua-3*, a gene required for mechanical tissue integrity in *Caenorhabditis elegans*, encodes a novel transmembrane protein of epithelial attachment complexes. *J Cell Biol*. 2001; 154:415–426. [PubMed: 11470828]
- Booij JC, Baas DC, Beisekeeva J, Gorgels TG, Bergen AA. The dynamic nature of Bruch's membrane. *Prog Retin Eye Res*. 2010; 29:1–18. [PubMed: 19747980]
- Bosher JM, Hahn BS, Legouis R, Sookhareea S, Weimer RM, Gansmuller A, Chisholm AD, Rose AM, Bessereau JL, Labouesse M. The *Caenorhabditis elegans* *vab-10* spectraplakins isoforms protect the epidermis against internal and external forces. *J Cell Biol*. 2003; 161:757–768. [PubMed: 12756232]
- Brenner S. The genetics of *Caenorhabditis elegans*. *Genetics*. 1974; 77:71–94. [PubMed: 4366476]
- Carbon S, Ireland A, Mungall CJ, Shu S, Marshall B, Lewis S. AmiGO: online access to ontology and annotation data. *Bioinformatics*. 2009; 25:288–289. [PubMed: 19033274]
- Carney TJ, Feitosa NM, Sonntag C, Slanchev K, Kluger J, Kiyozumi D, Gebauer JM, Coffin Talbot J, Kimmel CB, Sekiguchi K, et al. Genetic analysis of fin development in zebrafish identifies furin and hemicentin1 as potential novel fraser syndrome disease genes. *PLoS Genet*. 2010; 6:e1000907. [PubMed: 20419147]
- Dickinson DJ, Ward JD, Reiner DJ, Goldstein B. Engineering the *Caenorhabditis elegans* genome using Cas9-triggered homologous recombination. *Nat Methods*. 2013; 10:1028–1034. [PubMed: 23995389]
- Ding M, Goncharov A, Jin Y, Chisholm AD. *C. elegans* ankyrin repeat protein VAB-19 is a component of epidermal attachment structures and is essential for epidermal morphogenesis. *Development*. 2003; 130:5791–5801. [PubMed: 14534136]
- Dong C, Muriel JM, Ramirez S, Hutter H, Hedgecock EM, Breydo L, Baskakov IV, Vogel BE. Hemicentin assembly in the extracellular matrix is mediated by distinct structural modules. *The Journal of biological chemistry*. 2006; 281:23606–23610. [PubMed: 16798744]
- Edelstein A, Amodaj N, Hoover K, Vale R, Stuurman N. Computer control of microscopes using microManager. *Curr Protoc Mol Biol*. 2010 Chapter 14, Unit14 20.
- Feitosa NM, Zhang J, Carney TJ, Metzger M, Korzh V, Bloch W, Hammerschmidt M. Hemicentin 2 and Fibulin 1 are required for epidermal-dermal junction formation and fin mesenchymal cell migration during zebrafish development. *Dev Biol*. 2012; 369:235–248. [PubMed: 22771579]

- Gregory SL, Brown NH. kakapo, a gene required for adhesion between and within cell layers in *Drosophila*, encodes a large cytoskeletal linker protein related to plectin and dystrophin. *J Cell Biol.* 1998; 143:1271–1282. [PubMed: 9832555]
- Hagedorn EJ, Kelley LC, Naegeli KM, Wang Z, Chi Q, Sherwood DR. ADF/cofilin promotes invadopodial membrane recycling during cell invasion in vivo. *J Cell Biol.* 2014
- Hagedorn EJ, Sherwood DR. Cell invasion through basement membrane: the anchor cell breaches the barrier. *Curr Opin Cell Biol.* 2011; 23:589–596. [PubMed: 21632231]
- Hagedorn EJ, Yashiro H, Ziel JW, Ihara S, Wang Z, Sherwood DR. Integrin acts upstream of netrin signaling to regulate formation of the anchor cell's invasive membrane in *C. elegans*. *Dev Cell.* 2009; 17:187–198.
- Hagedorn EJ, Ziel JW, Morrissey MA, Linden LM, Wang Z, Chi Q, Johnson SA, Sherwood DR. The netrin receptor DCC focuses invadopodia-driven basement membrane transmigration in vivo. *J Cell Biol.* 2013; 201:903–913. [PubMed: 23751497]
- Hall DH, Hartwig E, Nguyen KC. Modern electron microscopy methods for *C. elegans*. *Methods Cell Biol.* 2012; 107:93–149.
- Hewitt RE, Powe DG, Holland CM, Gray T, Turner DR. Apparent fusion of basement membranes in colorectal carcinoma. *Int J Cancer.* 1992; 50:20–25. [PubMed: 1728609]
- Hong L, Elbl T, Ward J, Franzini-Armstrong C, Rybicka KK, Gatewood BK, Baillie DL, Bucher EA. MUP-4 is a novel transmembrane protein with functions in epithelial cell adhesion in *Caenorhabditis elegans*. *J Cell Biol.* 2001; 154:403–414. [PubMed: 11470827]
- Ihara S, Hagedorn EJ, Morrissey MA, Chi Q, Motegi F, Kramer JM, Sherwood DR. Basement membrane sliding and targeted adhesion remodels tissue boundaries during uterine-vulval attachment in *Caenorhabditis elegans*. *Nat Cell Biol.* 2011; 13:641–651. [PubMed: 21572423]
- Jefferson JJ, Leung CL, Liem RK. Plakins: goliaths that link cell junctions and the cytoskeleton. *Nat Rev Mol Cell Biol.* 2004; 5:542–553. [PubMed: 15232572]
- Kao G, Huang CC, Hedgecock EM, Hall DH, Wadsworth WG. The role of the laminin beta subunit in laminin heterotrimer assembly and basement membrane function and development in *C-elegans*. *Dev Biol.* 2006; 290:211–219. [PubMed: 16376872]
- Kefalides, NA.; Borel, JP. Basement membranes : cell and molecular biology. Elsevier Academic Press; Amsterdam ; San Diego: 2005.
- Kelley LC, Lohmer LL, Hagedorn EJ, Sherwood DR. Traversing the basement membrane in vivo: a diversity of strategies. *J Cell Biol.* 2014; 204:291–302. [PubMed: 24493586]
- Labouesse M. Role of the extracellular matrix in epithelial morphogenesis: a view from *C. elegans*. *Organogenesis.* 2012; 8:65–70. [PubMed: 22692230]
- Morf MK, Rimann I, Alexander M, Roy P, Hajnal A. The *Caenorhabditis elegans* homolog of the Opitz syndrome gene, *madd-2/Mid1*, regulates anchor cell invasion during vulval development. *Dev Biol.* 2013; 374:108–114. [PubMed: 23201576]
- Newman AP, White JG, Sternberg PW. Morphogenesis of the *C. elegans* hermaphrodite uterus. *Development.* 1996; 122:3617–3626. [PubMed: 8951077]
- Ozbek S, Balasubramanian PG, Chiquet-Ehrismann R, Tucker RP, Adams JC. The evolution of extracellular matrix. *Mol Biol Cell.* 2010; 21:4300–4305. [PubMed: 21160071]
- Ozzello L. The behavior of basement membranes in intraductal carcinoma of the breast. *Am J Pathol.* 1959; 35:887–899. [PubMed: 13670319]
- Rezniczek GA, de Pereda JM, Reipert S, Wiche G. Linking integrin alpha6beta4-based cell adhesion to the intermediate filament cytoskeleton: direct interaction between the beta4 subunit and plectin at multiple molecular sites. *J Cell Biol.* 1998; 141:209–225. [PubMed: 9531560]
- Roper K, Gregory SL, Brown NH. The 'spectraplakins': cytoskeletal giants with characteristics of both spectrin and plakin families. *J Cell Sci.* 2002; 115:4215–4225. [PubMed: 12376554]
- Seifert GJ, Lawson D, Wiche G. Immunolocalization of the intermediate filament-associated protein plectin at focal contacts and actin stress fibers. *Eur J Cell Biol.* 1992; 59:138–147. [PubMed: 1468436]
- Sherwood DR, Butler JA, Kramer JM, Sternberg PW. FOS-1 promotes basement-membrane removal during anchor-cell invasion in *C. elegans*. *Cell.* 2005; 121:951–962. [PubMed: 15960981]

- Sherwood DR, Sternberg PW. Anchor cell invasion into the vulval epithelium in *C. elegans*. *Dev Cell*. 2003; 5:21–31. [PubMed: 12852849]
- Srivastava A, Pastor-Pareja JC, Igaki T, Pagliarini R, Xu T. Basement membrane remodeling is essential for *Drosophila* disc eversion and tumor invasion. *Proceedings of the National Academy of Sciences of the United States of America*. 2007; 104:2721–2726. [PubMed: 17301221]
- Sulston JE, White JG. Regulation and cell autonomy during postembryonic development of *Caenorhabditis elegans*. *Dev Biol*. 1980; 78:577–597. [PubMed: 7190941]
- Thompson CL, Klein BE, Klein R, Xu Z, Capriotti J, Joshi T, Leontiev D, Lee KE, Elston RC, Iyengar SK. Complement factor H and hemicentin-1 in age-related macular degeneration and renal phenotypes. *Hum Mol Genet*. 2007; 16:2135–2148. [PubMed: 17591627]
- Tsuji N, Kita K, Ozaki K, Narama I, Matsuura T. Organogenesis of mild ocular coloboma in FLS mice: failure of basement membrane disintegration at optic fissure margins. *Exp Eye Res*. 2012; 94:174–178. [PubMed: 22182670]
- Vaccaro CA, Brody JS. Structural features of alveolar wall basement membrane in the adult rat lung. *Journal of Cell Biology*. 1981; 91:427–437. [PubMed: 7198126]
- Vogel BE, Hedgecock EM. Hemicentin, a conserved extracellular member of the immunoglobulin superfamily, organizes epithelial and other cell attachments into oriented line-shaped junctions. *Development*. 2001; 128:883–894. [PubMed: 11222143]
- Whittaker CA, Hynes RO. Distribution and evolution of von Willebrand/integrin A domains: widely dispersed domains with roles in cell adhesion and elsewhere. *Mol Biol Cell*. 2002; 13:3369–3387. [PubMed: 12388743]
- Xu X, Dong C, Vogel BE. Hemicentins assemble on diverse epithelia in the mouse. *J Histochem Cytochem*. 2007; 55:119–126. [PubMed: 17015624]
- Yurchenco PD. Basement membranes: cell scaffoldings and signaling platforms. *Cold Spring Harb Perspect Biol*. 2011:3.
- Zhang H, Landmann F, Zahreddine H, Rodriguez D, Koch M, Labouesse M. A tension-induced mechanotransduction pathway promotes epithelial morphogenesis. *Nature*. 2011; 471:99–103. [PubMed: 21368832]
- Ziel JW, Hagedorn EJ, Audhya A, Sherwood DR. UNC-6 (netrin) orients the invasive membrane of the anchor cell in *C. elegans*. *Nat Cell Biol*. 2009; 11:183–U161. [PubMed: 19098902]

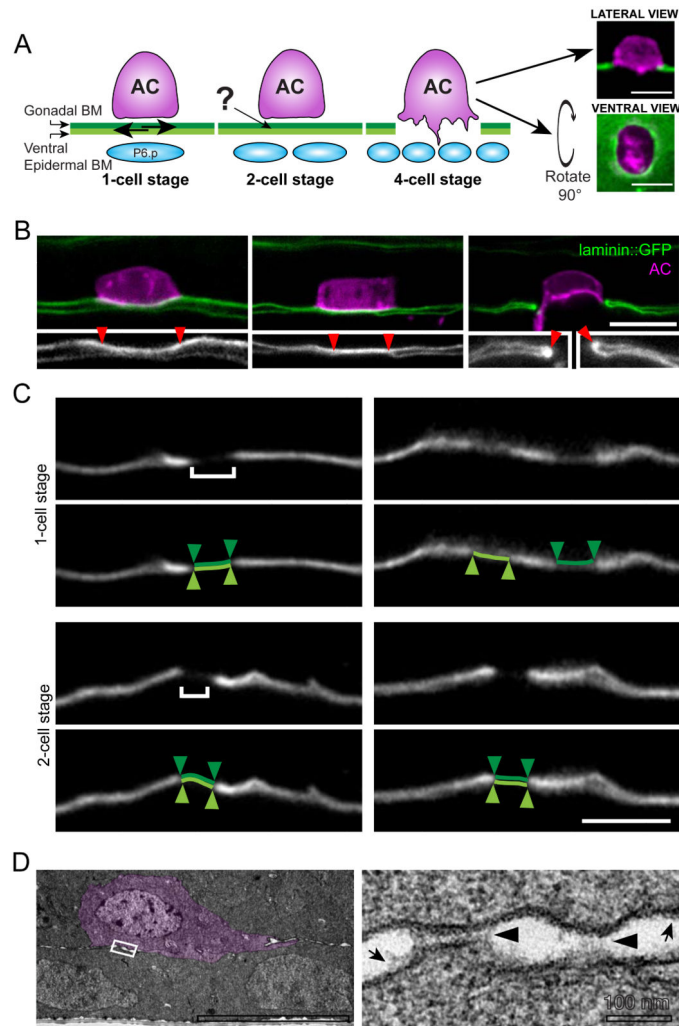


### Figure 1. The gonadal and ventral epidermal BMs are linked prior to AC invasion

(A) During the P6.p one-cell stage the gonadal (dark green) and ventral epidermal (light green) BMs are unattached and shift in their position (arrows, left). The AC invades at the late P6.p two-cell stage and the BMs fuse on either side of the AC following invasion (P6.p four-cell stage). How the AC coordinates invasion across two BMs is unknown (see ?). The BM (laminin::GFP, green) and the AC (*cdh-3* > mCherry::moeABD, magenta) can be visualized from a lateral perspective (top) or from a ventral perspective (bottom). (B) onfocal images of worms at the early P6.two-cell stage with slightly separated gonadal and ventral BMs show that the BM under the AC (marked between arrowheads in 2X magnified inset) can be resolved as two separate structures (left). These BMs are not resolvable as two distinct sheets just prior to invasion (middle) and fuse on either side of the AC following invasion (right, arrowheads in inset, n=13/24 two-cell stage animals with linked BMs; 19/19 four-cell stage worms with fused BMs). (B) Worms at the P6.p one-cell stage and P6.p two-cell stage were laterally shifted to induce tissue misalignment (see Methods). At the one-cell stage (top), photobleached regions (brackets, left) of gonadal and ventral BM (white; photobleached region highlighted in light and dark green below) were no longer aligned post-shift (n=4/8 animals, right). At the two-cell stage, the photobleached regions remained



aligned after tissue shifting (n=9/9, bottom). (D) Transmission electron micrographs of the AC (pseudocolored in magenta) reveal punctate structures (black arrowheads, right) spanning the gonadal and ventral BMs (n=4/5 P6.p two-cell stage worms). Arrows highlight the BMs, which closely adjoin the cell membranes. The boxed area on the left image is shown at higher magnification on the right. Scale bars, 5 $\mu$ m. See also Figure S1.

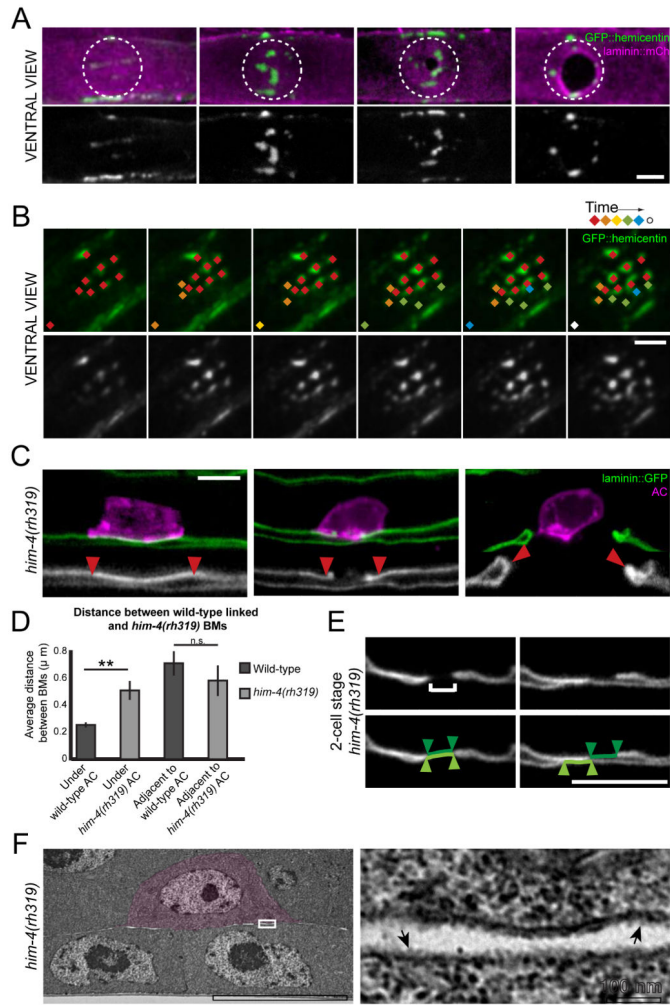


### Figure 2. Hemicentin is required for BM-BM adherence

(A) A ventral perspective of the BM shows GFP::hemicentin (green, top; white, bottom) in punctate accumulations in the BM (laminin::mCherry, magenta) specifically under the AC (dashed circle) beginning at the P6.p one-cell stage (left). Hemicentin punctae are pushed aside as the AC invades through the BM, forming a ring at the edge of the BM gap (right). (B) Nascent hemicentin accumulations (green, top; white, bottom) are marked with a new color at 10 min intervals to highlight their stability. This animal corresponds to Movie S1. (C) Worms in which the gonadal and ventral BMs could be resolved reveal that the BMs are not adherent in hemicentin mutant (*him-4(rh319)*) animals prior to (mid P6.p two-cell stage) or during invasion (P6.p four-cell stage; n=10 animals). Insets are 2- fold magnifications and arrowheads delineate the BMs under the AC. The BMs in hemicentin mutants fuse following invasion (right, arrowheads, inset; n=10 animals). (D) Graph shows the average distance between the gonadal and ventral BM in wild-type worms and *him-4(rh319)* worms underneath the AC and adjacent to the AC (n = 10 animals analyzed for each group, \*\*p<0.005, Students *t*-test, error bars represent SEM) (E) A small region of the BMs (laminin::GFP, white) under the AC of *him-4(rh319)* animals at the mid two-cell stage was photobleached (brackets, left). Following tissue shift, the photobleached regions of the

gonadal BM (highlighted in dark green) and the ventral BM (highlighted in light green) were no longer aligned (n=3/4, right). (E) Transmission electron micrographs of *him-4(rh319)* animals with the AC highlighted in magenta reveal an absence of structures (boxed area at higher magnification, right) spanning the gonadal and ventral BMs (arrows, n=4/4). Scale bars, 5 $\mu$ m. See also Figure S2.

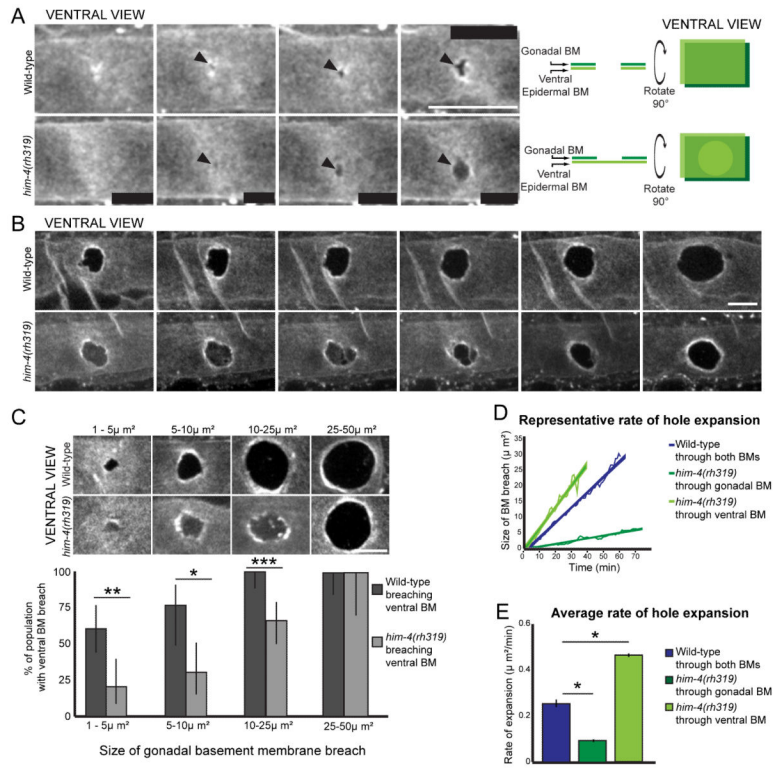


**Figure 3. Hemicentin mutants have delayed ventral epidermal BM breaching**  
 (A) Time-lapse analysis of wild-type worm shows breach of both the gonadal and ventral BMs (laminin::GFP, white; arrowheads, top). In contrast, a *him-4(rh319)* worm at the P6.p two-cell stage (bottom) initially breaches only the gonadal BM (arrowheads, note the GFP signal present from ventral BM). The diagram on the right schematically depicts this data from both the lateral and ventral perspective. (B) Time-lapse analysis of a wild-type worm (top) and *him-4(rh319)* worm (bottom) reveals that the *him-4* mutant breaches the ventral BM in a delayed manner at the P6.p four-cell stage (images correspond with Movie S3). (C) Ventral BM breach assessed in relation to gonadal breach. Representative images of each category are pictured. (\* $p < 0.05$ , \*\* $p < 0.005$ , \*\*\* $p < 0.0005$ , 17 animals for each category, Fisher's exact test, error bars denote 95% confidence intervals with a continuity correction). (D) The graph depicts BM removal in representative animals. (E) The average rate of BM opening (\* $p < 0.05$ , Student's *t*-test, 7 timelapses for each category, error bars represent SEM). Scale bars, 5  $\mu\text{m}$ . See also Figure S3.

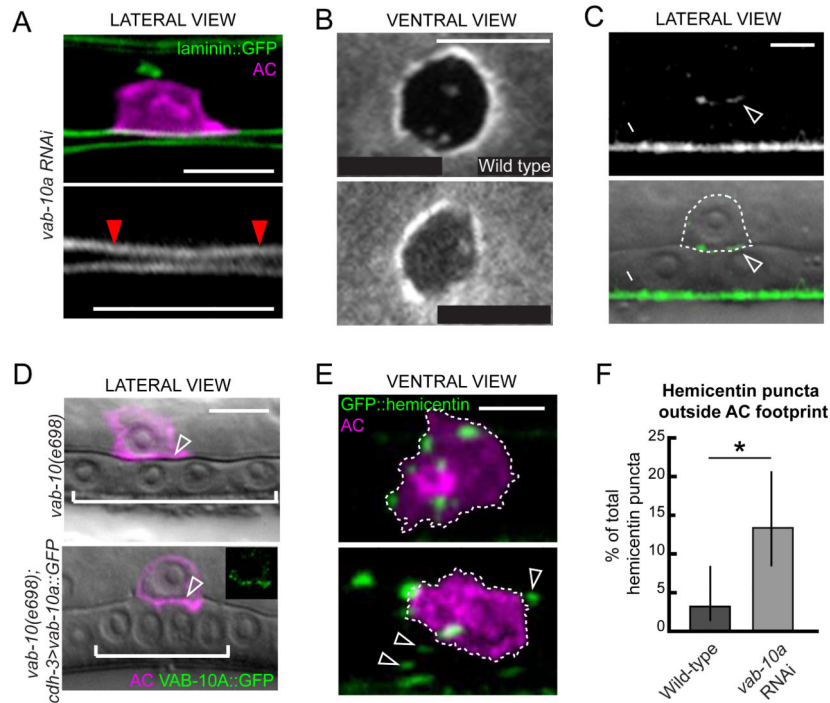


#### Figure 4. AC expressed VAB-10A/plakin is required for BM-BM adhesion

(A) An animal treated with *vab-10a* RNAi shows a lack of adhesion between the gonadal and ventral BMs (laminin::GFP, green, top; white, bottom) under the AC (mCherry::PLC $\delta^{\text{PH}}$ , magenta) prior to invasion (red arrowheads delineate BM under the AC, distance between BMs= $0.61 \pm 0.01$ ,  $n=9$ ,  $p < 0.0005$  compared to wild-type, Student's *t*-test). (B) A ventral perspective of laminin::GFP in a wild-type (top) and *vab-10a* RNAi treated animal (bottom) shows delayed ventral BM breach after reduction of *vab-10a* (indicated by increased signal under AC, see Figure 3A for schematic; 19/23 animals with 1-5  $\mu\text{m}^2$  gonadal BM holes fail to breach ventral BM,  $p < 0.005$  compared to wild-type, Fisher's exact test). (C) GFP inserted in frame in the *vab-10a* genomic locus revealed that VAB-10A::GFP accumulates at the AC-BM interface (arrowhead, fluorescence top, overlaid on DIC, bottom, AC outlined with dashed line), and the site of epidermal-cuticle contact (arrow). (D) A DIC image overlaid with a marker for the AC (mCherry::PLC $\delta^{\text{PH}}$ , magenta) shows a *vab-10(e698)* mutant (top) that failed to invade (BM is not breached as indicated by intact phase-dense line, arrowhead). Expression of VAB-10A in the AC (*cdh-3>vab-10a::GFP*, inset) rescued the invasion defect (arrowhead indicates BM breach;  $n=41/44$  animals with complete invasion). (E) Hemicentin punctae (green) are contained within the region of AC-BM contact (outlined by dotted line, AC in magenta). Following treatment with RNAi targeting *vab-10a*, the hemicentin punctae were no longer contained within the AC footprint (bottom, arrowheads). (F) The graph quantifies the percentage of punctae in wild-type and *vab-10* RNAi treated animals outside the AC footprint (\* $p < 0.05$ , Fisher's exact test, 100 animals for each treatment, error bars show 95% confidence interval with a continuity correction). Scale bars, 5 $\mu\text{m}$ . See also Figure S4.

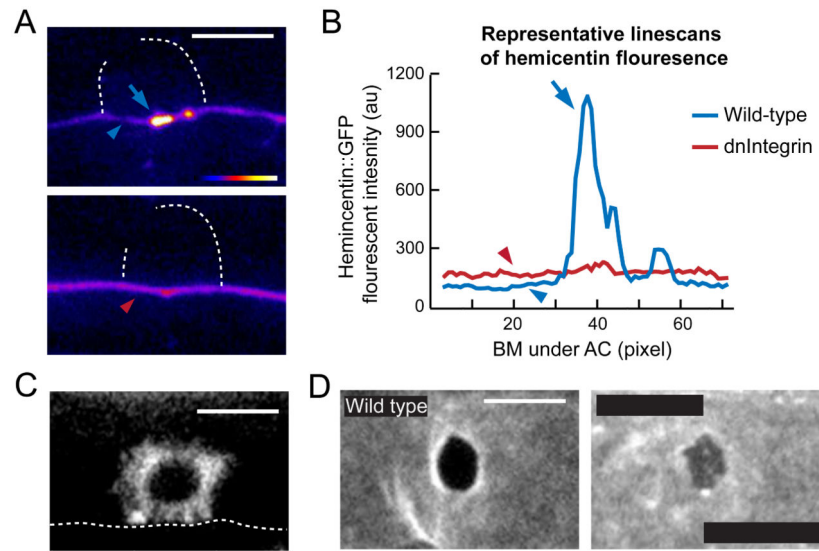


**Figure 5. INA-1/PAT-3 integrin is required for the formation of hemicentin punctae**  
 (A) Spectral representation of GFP::hemicentin fluorescence intensity shows high concentrations of hemicentin in punctae (blue arrow) and low levels in the surrounding BM in a wild-type animals under the AC (blue arrowhead). An animal expressing AC-specific dominant-negative integrin, which disrupts the function of the INA-1/PAT-2 heterodimer (*zmp-1>HA-βtail*), shows diffuse hemicentin but no punctae under the AC (red arrowhead). (B) Linescans of BM-localized GFP::hemicentin in wild-type and *HA-βtail* animals under the AC show peak in expression at a hemicentin punctae in a wild-type animal (blue arrow), and slightly elevated levels of hemicentin in the surrounding BM after reduction of integrin (compare red and blue arrowheads; n=11 *zmp-1>HA-βtail* and 18 wild-type animals; see also Figure S4). (C) AC-specific dominant negative integrin (*zmp-1>HA-βtail*) disrupted the polarity of VAB-10A::GFP (*cdh-3>VAB-10A::GFP*) at the AC-BM interface (dotted line; n=7/8 worms examined). (D) Ventral view of BM breach shows a wild-type animal (top) that has breached both the gonadal and ventral BMs, while the animal treated with *ina-1* RNAi (bottom, integrin α subunit) breached the gonadal, but not the ventral BM (12/14 animals with 1-5 μm<sup>2</sup> gonadal BM holes fail to breach ventral BM, p<0.005 compared to wild-type, Fisher's exact test;). Scale bars, 5μm. See also Figure S5.

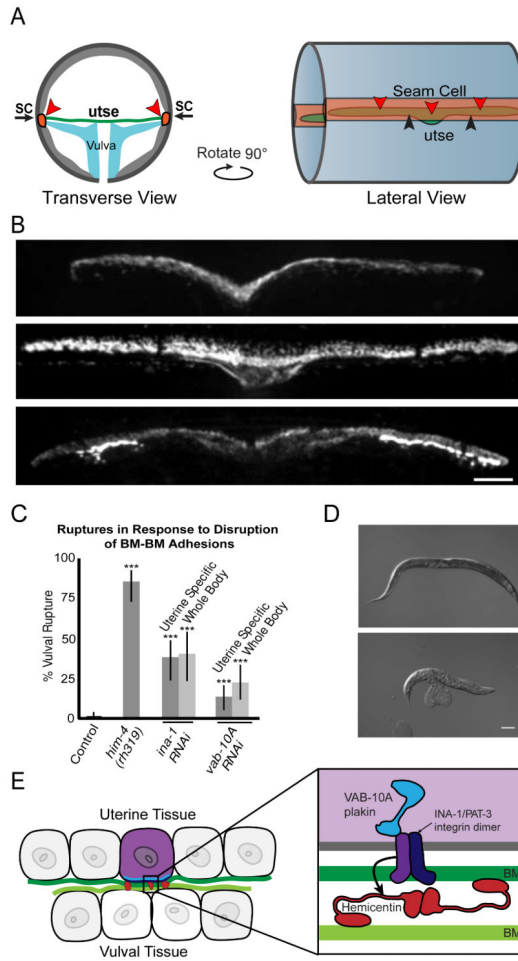


**Figure 6. The uterine-seam attachment is regulated by hemicentin, VAB-10A and integrin**  
 (A) Structure of the attachment between the uterine utse and epidermal seam cells (SC) in transverse (left) and lateral (right) views. Red arrowheads denote location of adherent BMs.  
 (B) Fluorescence images showing localization of GFP::hemicentin (top), VAB-10A::GFP (middle), and integrin (INA-1; PAT-3::GFP, bottom) in the utse. Scale bar, 5µm.  
 (C) Graph depicts percent of worms ruptured through the vulva in *him-4(rh319)* and following RNAi knockdown of *ina-1* or *vab-10a* in the entire body (*rrf-3(pk1426)*) or specifically the uterine tissue (*qyIs103(fos-1a>rde-1); rde-1(ne219); rrf-3(pk1426)*); \*\*\**p*<0.0005 compared to control by Fisher's exact test, error bars denote 95% confidence intervals with a continuity correction, n = 40 animals for each category). (D) Images of a wild-type worm and a *him-4(rh319)* mutant with a prolapsed uterus. Scale bar, 100 µm. (E) A schematic diagram of a B-LINK adhering the uterine and vulval tissues through their adjacent BMs prior to AC invasion. Intracellular VAB-10A/plakin (blue) and the integrin heterodimer INA-1/PAT-3 (purple) are found at the basal surface of the AC while hemicentin (red) is localized in punctae between the gonadal and ventral BMs beneath the AC.

Table 1

## Efficiency of AC invasion

Genotype/Treatment	%No Invasion	% Partial Invasion	% Complete Invasion	n=
<b>Screen of hemidesmosome components<sup>a</sup></b>				
<i>L4440</i> (empty vector)	0	0	100	40
<i>him-4</i> (RNAi)	18	16	66	50
<i>vab-10</i> ( <i>e698</i> )	13	22	65	69
<i>vab-10a</i> (RNAi)	8	15	78	40
<i>vab-10b</i> (RNAi)	0	2	98	50
<i>git-1</i> ( <i>tm1962</i> )	0	0	100	50
<i>git-1</i> (RNAi)	0	4	96	50
<i>let-805</i> (RNAi)	0	0	100	25
<i>mua-3</i> ( <i>rh195</i> )	0	0	100	25
<i>mua-3</i> (RNAi)	3	8	89	65
<i>mup-4</i> (RNAi)	0	5	95	22
<i>pak-1</i> ( <i>ok448</i> )	0	0	100	40
<i>pak-1</i> (RNAi)	0	0	100	21
<i>pix-1</i> ( <i>gk416</i> )	0	0	100	25
<i>eps-8</i> ( <i>ok539</i> )	0	0	100	27
<i>eps-8</i> (RNAi)	0	0	100	50
<i>vab-19</i> ( <i>e1036</i> )	0	6	94	53
<b>Site of Action Experiments</b>				
<b>Uterine specific RNAi</b>				
<i>vab-10a</i> (RNAi); <i>qyIs103</i> ( <i>fos-1a&gt;rde-1</i> ); <i>rde-1</i> ( <i>ne219</i> ); <i>rrf-3</i> ( <i>pk1426</i> )	20	14	66	50
<b>Vulval specific RNAi</b>				
<i>vab-10a</i> (RNAi); <i>mfls70</i> ( <i>lin-31&gt;rde-1</i> ); <i>rde-1</i> ( <i>ne219</i> ); <i>rrf-3</i> ( <i>pk1426</i> )	0	3	97	94
<b>AC rescue</b>				
<i>cdh-3&gt;vab-10a::GFP</i> ; <i>vab-10</i> ( <i>e698</i> )	0	7	93	44
<i>cdh-3&gt;vab-10aAPRD::GFP</i> ; <i>vab-10</i> ( <i>e698</i> )	18	18	63	49
<b>Secondary screen of intermediate filaments<sup>b</sup></b>				
<i>L4440</i> (empty vector)	2	1	97	100
<i>ifb-2</i> (RNAi)	0	4	96	48
<i>ifc-2</i> (RNAi)	1	1	98	79
<i>ifd-1</i> (RNAi)	0	1	99	85
<i>ifd-2</i> (RNAi)	5	4	91	100
<i>ifc-2</i> (RNAi); <i>ifd-1</i> (RNAi); <i>ifd-2</i> (RNAi)	7	7	86	100
<b><i>him-4</i> and <i>vab-10a</i> genetic interaction</b>				
<i>him-4</i> ( <i>rh319</i> )	19	17	64	178
<i>vab-10a</i> (RNAi); <i>him-4</i> ( <i>rh319</i> )	14	16	70	193



<sup>a</sup>RNAi screen was conducted in the *rrf-3(pk1426); qyIs7(laminin::GFP)* background.

<sup>b</sup>RNAi screen was conducted in the *rrf-3(pk1426); rhIs23(GFP::hemicentin)* background. *rrf-3* mutants are more sensitive to somatic RNAi effects.